

Vortex Pinning in Neutron Stars, Slip-stick Dynamics, and the Origin of Spin Glitches

BENNETT LINK¹ AND YURI LEVIN^{2,3,4}

¹*Department of Physics, Montana State University, Bozeman, MT 59717, USA*

²*Physics Department and Columbia Astrophysics Laboratory, Columbia University, 538 West 120th Street New York, NY 10027, USA*

³*Center for Computational Astrophysics, Flatiron Institute, 162 Fifth Avenue, New York, NY 10010, USA*

⁴*Department of Physics and Astronomy, Monash University, Clayton VIC 3800, AUSTRALIA*

ABSTRACT

We study pinning and unpinning of superfluid vortices in the inner crust of a neutron star using 3-dimensional dynamical simulations. Strong pinning occurs for certain lattice orientations of an idealized, body-centered cubic lattice, and occurs generally in an amorphous or impure nuclear lattice. The pinning force per unit length is $\sim 10^{16}$ dyn cm⁻¹ for a vortex-nucleus interaction that is repulsive, and $\sim 10^{17}$ dyn cm⁻¹ for an attractive interaction. The pinning force is strong enough to account for observed spin jumps (glitches). Vortices forced through the lattice move with a slip-stick character; for a range of superfluid velocities, the vortex can be in either a cold, pinned state or a hot unpinned state, with strong excitation of Kelvin waves on the vortex. This two-state nature of vortex motion sets the stage for large-scale vortex movement that creates an observable spin glitch. We argue that the vortex array is likely to become tangled as a result of repeated unpinning and repinnings. We conjecture that during a glitch, the Kelvin-wave excitation spreads rapidly along the direction of the mean superfluid vorticity and slower in the direction perpendicular to it, akin to an anisotropic deflagration.

1. INTRODUCTION

Spin glitches are ubiquitous in neutron stars (NSs), seen in radio pulsars, x-ray pulsars, magnetars, and millisecond pulsars. Typical glitches show a fractional change in spin rate of 10^{-8} to 10^{-6} . The spin-up portion of a glitch has never been fully time resolved; the remarkable 2016 spin glitch of the Vela pulsar of magnitude $\Delta\nu/\nu = 1.4 \times 10^{-6}$, occurred in under 12.6 s (Ashton et al. 2019), suggestive of a localized, mechanical process. The most prolific glitching NS is the x-ray pulsar J0537-6910, which has suffered 45 glitches in 13 years (Antonopoulou et al. 2017). Glitches produce observable changes of the pulsar magnetosphere (Ashton et al. 2019; Palfreyman et al. 2016); see Bransgrove et al. (2020) for discussion.

Glitches are thought to represent sudden coupling between the NS crust, whose spin rate we directly observe, and the interior superfluid. The angular momentum of the superfluid is determined by the distribution of quantized vortex lines, which are predicted to pin to the nuclei of the inner crust (Anderson & Itoh 1975; Alpar 1977; Epstein & Baym 1988; Link & Epstein 1991; Pizzochero et al. 1997; Donati & Pizzochero 2004, 2006, 2003; Avogadro et al. 2007, 2008; Link 2009), the region of the star with mass density between the nuclear drip density (average density in baryons, including nuclei) of $\simeq 2.4 \times 10^{-4}$ fm⁻³ ($\simeq 4 \times 10^{11}$ g cm⁻³) to about half nuclear density, $\sim 7 \times 10^{-2}$ fm⁻³ ($\sim 10^{14}$ g cm⁻³). As the star spins down under external torque, vortex pinning fixes the angular velocity of a portion of the superfluid, storing angular momentum in the region with pinning, while a hydrodynamic lift force (Magnus force) gradually increases on the pinned vortices. As a consequence of an unidentified instability, a significant fraction of the $\sim 10^{17}$ vortices in the inner crust unpin and moves *en masse*. The vortices then drag against the crust, driving a spin jump. A possible trigger of vortex unpinning is the inevitable structural relaxation of the crust (a starquake) as the star spins down that triggers vortex motion, by moving vortices with the matter Ruderman (1991), or causing vortices to unpin directly (Alpar et al. 1996), or locally heating the crust and mobilizing many vortices through thermal activation Link & Epstein (1996). Another possibility is that large-scale unpinning is the result of a vortex avalanche, wherein an unpinned vortex segment approaches a pinned vortex segment, causing it to unpin - each unpinned vortex unpins another vortex and an avalanche develops (Cheng et al. 1988; Warszawski & Melatos 2008, 2011; Warszawski et al. 2012; Warszawski & Melatos 2013; Howitt et al. 2020).

The available angular momentum stored in the superfluid for driving a spin glitch is determined by the strength to which the vortices pin to the nuclear lattice. Pinning occurs as a dynamical relaxation process. A vortex forced through the lattice against drag will fall into local minima of the interaction potential, exciting waves on the vortex. As the waves damp (*e. g.*, through the excitation of lattice and superfluid phonons), the vortex assumes a shape that strikes a compromise between the energy gain of falling into local minima of the lattice potential and the energy cost of bending the vortex (which increases its length). Many different metastable pinning states are possible, so the actual pinned state a vortex finds will depend on initial conditions. The strength of pinning will be determined by: i) the basic interaction between a vortex and a nucleus, ii) the lattice structure, and the iii) tension (self-energy) of a vortex. A vortex will pin to nuclei if the vortex-nucleus interaction is attractive, and to the interstices of the lattice if the interaction is repulsive.

There has been substantial disagreement over the magnitude and sign of the vortex-nucleus interaction in the inner crust. Quantum calculations (using a mean-field Hartree-Fock-Bogoliubov formulation) show a repulsive interaction with an energy of up to ~ 3 MeV (Avogadro et al. 2007, 2008) throughout the inner crust, while semi-classical calculations (using a local density approximation) show a repulsive interaction of $\sim 1 - 2$ MeV below an average baryon density of $\sim 10^{-2} \text{ fm}^{-3}$ ($\sim 2 \times 10^{13} \text{ g cm}^{-3}$) which turns attractive with a strength of ~ 5 MeV at higher densities (Pizzochero et al. 1997; Donati & Pizzochero 2003, 2004, 2006). A step toward resolving the controversy was made by Wlazłowski et al. (2016), using density functional theory (in principle, an exact approach); they find that the vortex-nucleus interaction is always repulsive in the average baryon density range 0.02 fm^{-3} ($3 \times 10^{13} \text{ g cm}^{-3}$) to 0.04 fm^{-3} ($7 \times 10^{13} \text{ g cm}^{-3}$), with a force of $\sim 1 \text{ MeV fm}^{-1}$ over a range of $\sim 4 \text{ fm}$, corresponding to an interaction energy per nucleus of $\sim 4 \text{ MeV}$.

The ground state of a single-component Coulomb lattice is a body-centered-cubic (bcc) structure. In a bcc lattice, the pinned vortex will consist of segments that follow the lattice planes, separated by kinks that traverse the lattice planes, producing some degree of frustration of the pinned vortex. As a Magnus force is applied, the kinks will move. Jones (1997) argues that the kinks move easily, so that pinning to a regular lattice would be very weak.

The inner crust, though, is probably not an ideal bcc lattice. Jones (1999, 2001) has shown that thermal fluctuations will cause the crust to solidify with variations in the nuclear charge and lattice defects (*i. e.*, missing nuclei or mono-vacancies), that destroy long-range order and most likely make the crust into a glass.¹ Kobayakov & Pethick (2014) have shown that, above the neutron drip density, interstitial neutrons give rise to an attractive force between nuclei that renders a bcc lattice unstable. Kobayakov & Pethick (2014) suggest that the lattice structure is that of a superlattice with, *e. g.*, two nuclei per unit cell, analogous to ferroelectric materials such as BaTiO_3 , but such a lattice might never be realized according to the arguments of Jones (1999, 2001).

The first three-dimensional simulations of vortex motion in a nuclear lattice were performed by Link (2009) for a nuclear glass using a classical treatment of the vortex motion and parameterized potential for the vortex-nucleus interaction. Assuming that the range of the potential is equal to the lattice spacing, Link (2009) found that pinning occurs with equal strength, independent of the sign of the interaction. All pinning calculations described above show that the range of the vortex-nucleus interaction is typically smaller than the lattice spacing, and calculations in this regime are needed, as we present here. Wlazłowski et al. (2016) performed three-dimensional dynamical simulations using density functional theory to obtain the vortex-nucleus interaction; these calculations considered a vortex interacting with a single nucleus and so did not address lattice effects. Here we use a new numerical algorithm to study vortex pinning and unpinning with three-dimensional dynamical simulations, considering different possibilities for the structure of the nuclear lattice. We evaluate the vortex pinning force, and identify a slip-stick character to vortex motion that could play a role in pulsar glitches.

2. VORTEX EQUATION OF MOTION

We treat a vortex classically as a string with tension at zero temperature. Let the vortex shape, measured with respect to the z axis, be given by the two-dimensional displacement vector $\mathbf{u}(z, t) = \hat{x}u_x + \hat{y}u_y$. For small bending angles, so that $|\partial\mathbf{u}/\partial z| \ll 1$, the equation of motion is (Schwarz 1977, 1978)

$$T_v \frac{\partial^2 \mathbf{u}}{\partial z^2} + \rho_s \boldsymbol{\kappa} \times \left(\frac{\partial \mathbf{u}}{\partial t} - \mathbf{v}_s \right) - \eta \frac{\partial \mathbf{u}}{\partial t} + \mathbf{f} = 0, \quad (1)$$

¹ A highly impure crust would have low thermal conductivity, and is disfavored by observations of the thermal response of the crust following an episode of accretion (Brown & Cumming 2009).

The first term is the force (per unit length) from bending the vortex; T_v is the vortex tension. The second term is the Magnus force; ρ_s is the (unentrained) superfluid mass density, $\boldsymbol{\kappa}$ is the local vorticity vector, and \mathbf{v}_s is the external superfluid flow velocity. The third term is the drag force due to motion of the vortex with respect to the nuclear lattice; η is the drag coefficient. The last term \mathbf{f} is the force due to interaction of the vortex with the nuclear lattice. The effects of vortex inertia are negligible, so the velocity of any point on the vortex is determined entirely by the net force at that point and by the shape of the vortex. All forces are perpendicular to the vortex. We solve this equation using a new spectral method described in the Appendix A. Given the uncertainties in the vortex-nucleus interaction, we model the potential parametrically for different possible lattice structures; details are given in Appendix B.

The dominant damping process of vortex motion occurs through the excitation of Kelvin waves on the vortex (Epstein & Baym 1992; Jones 1992), which then exchange energy with lattice phonons. While our treatment accounts for the excitation of Kelvin waves, we do not treat the excitation of lattice phonons explicitly; the latter process is treated with the drag term in eq. 1. The drag coefficient is typically $\gamma \equiv \eta/\rho_s\kappa \sim 10^{-3}$ for a vortex that is moving quickly through the lattice (Epstein & Baym 1992; Jones 1992), so Kelvin waves are underdamped.² Calculations for $\gamma \ll 1$ require long run times; we fix $\gamma = 0.1$ to keep computation times tractable, while remaining in the expected underdamped regime. The way in which a vortex unpins and repins probably has some dependence on γ , which we do not study here.³

3. RESULTS OF DYNAMICAL SIMULATIONS

3.1. Bcc lattice

To illustrate the effects of lattice structure on vortex pinning and unpinning, we begin with an ideal bcc lattice. For the potential, we take

$$V(\mathbf{r}, t) = \frac{E_p}{b} \exp \left[-\frac{b}{\sigma_p} \sum_{i=1}^3 \sin^2 \left(\pi \hat{e}_i \cdot \frac{\mathbf{r}}{b} \right) \right] \quad (2)$$

where E_p is the interaction energy per nucleus, b is the lattice spacing, σ_p is the length scale of the interaction, and \hat{e}_i are orthonormal lattice vectors. The force per unit length near a nucleus scales as σ_p^{-1} , distributed over a segment of the vortex of length σ_p , so the critical force for unpinning is nearly independent of σ_p for the regime of interest with $\sigma_p \ll b$, scaling as $b^{-2}E_p$.

To determine the threshold for unpinning, we first choose a set of lattice vectors for the bcc lattice, and then let the vortex relax dynamically to a pinned configuration with zero external superfluid flow. We then increase the superfluid flow velocity v_s adiabatically. (If v_s is increased too abruptly, waves are excited on the vortex that cause it to unpin.) The vortex remains pinned to a threshold value of v_s . Typically, as v_s is increased, the vortex undergoes some adjustment that strengthens its position, allowing it to remain pinned. As v_s is further increased, the vortex unpins and starts moving through the lattice, and Kelvin waves are excited on the vortex. After further increase of v_s , the vortex enters a ballistic regime in which the tension and pinning terms in eq. 1 average to nearly zero. The solution to eq. 1 in this regime to first order in small $\gamma \equiv \eta/\rho_s\kappa$ is

$$\frac{\partial \mathbf{u}}{\partial t} \simeq v_s(\hat{x} - \gamma \hat{y}). \quad (3)$$

The vortex moves at an angle $\simeq \gamma$ with respect to the direction of the applied flow. The superfluid velocity is then slowly decreased to zero; the vortex repins and stops. A movie of the motion is shown in Fig. 1.

[Click here for animation](#)

Figure 1. Animation of a vortex forced through an attractive bcc lattice. The translational motion has been subtracted. The vortex is 100 lattice units long along the z axis; the x and y axis have been scaled up by a factor of 10. The lattice vectors are $\hat{e}_1 = [0, 0, 1]$, $\hat{e}_2 = [0, 1/2, 1/2]$, $\hat{e}_3 = [0, -1/2, 1/2]$. The force is in the y direction, decreasing from zero until $t = 500$, and then decreasing back to zero by $t = 1000$. The initial, pinned vortex, obtained by letting the vortex damp to the lattice with no external force (not shown), generally follows a lattice plane, with jogs and kinks. As the force is increased, the vortex eventually becomes unstable and becomes excited with helical waves. As the force is reduced, the vortex repins in a different configuration than the initial one.

² For low-velocity motion ($v_s < 10^3$ cm s⁻¹), Jones (1990) finds $\gamma \sim 10^{-5} - 10^{-4}$. That calculation assumes that vortices cannot pin, while we find that vortices pin strongly in this regime.

³ We find the dependence on γ to be weak in the interval $0.03 < \gamma < 0.3$.

We find that pinning depends strongly on the lattice orientation, as predicted by Jones (1997). For most lattice angles the pinning is very strong, and for some pinning is virtually nonexistent. The lack of effective pinning for some lattice angles is due to the presence of kinks in equilibrium configurations that have very high mobility. Examples of vortex response are shown in Fig. 2. Performing many simulations for different E_p , and averaging over randomly chosen lattice orientations for each value of E_p , we find a pinning force per unit length for an attractive pinning potential of

$$f_p \simeq \frac{2 \times 10^{-3}}{3 \times 10^{17}} \left(\frac{|E_p|}{4 \text{ MeV}} \right) \left(\frac{b}{30 \text{ fm}} \right)^{-2} \begin{array}{l} \text{MeV fm}^{-2} \\ \text{dyn cm}^{-1} \end{array} \quad (4)$$

By comparison, the strongest possible pinning occurs for a lattice that is aligned with the vortex. The pinning force per unit length is then, for the fiducial values above, $f_p \sim b^{-2} E_p \sim 4 \times 10^{-3} \text{ MeV fm}^{-2} \simeq 7 \times 10^{17} \text{ dyn cm}^{-1}$. The angle-averaged pinning force above is nearly this strong, since pinning occurs for most lattice orientations. Our estimate for the pinning strength in eq. 4 is ~ 300 times larger than found by Seveso et al. (2016), and a factor of 3-30 smaller than estimated by Anderson & Itoh (1975) with a dimensional argument.

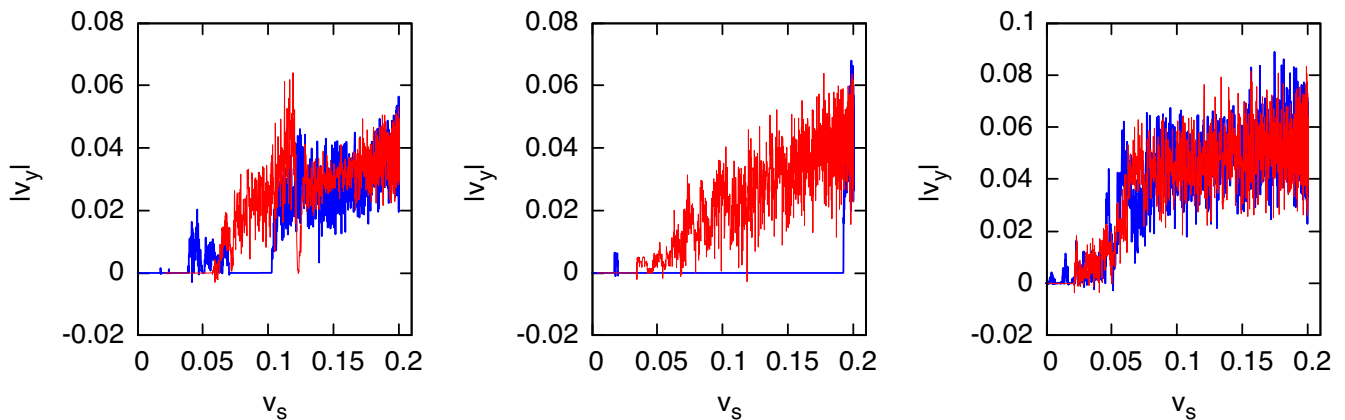


Figure 2. Unpinning/repinning transitions in an attractive bcc lattice for three arbitrary lattice orientations; shown is vortex speed in the $-\hat{y}$ direction versus applied superfluid flow velocity v_s in the \hat{x} direction. For the blue (red) curves the force is increasing (decreasing) with time. In the leftmost figure, the vortex undergoes some adjustment as the force is increased, before unpinning suddenly at $v_s \sim 0.1$. Above this velocity, the vortex enters a ballistic regime. As the Magnus force is lowered, the vortex does not repin until v_s is significantly less than the threshold for unpinning, a strong hysteresis effect. The rightmost figure shows a rare example for which there is not a strong unpinning transition. The parameters are $E_p = -4 \text{ MeV}$, $b = 30 \text{ fm}$, $\sigma_p = .3b$. Velocity units are $T_v/\rho_s \kappa b \sim 2 \times 10^8 \text{ cm s}^{-1}$.

We note the presence of strong hysteresis in the vortex response to the force; the vortex typically repins at a much lower value of v_s than the value at which it unpinning. The reason for this effect is that the unpinning vortex has a high effective temperature, with continuous excitation of Kelvin waves that inhibit repinning, while the immobile (cold) vortex is able to dig into the pinning potential. The vortex thus has *two distinct states for the same applied force* - one pinned, the other unpinning - and the vortex motion acquires a *slip-stick* character. This slip-stick character of vortex motion is generally present, with the repinning value of v_s significantly smaller than the unpinning value, but is absent for special lattice orientations. This feature of vortex motion arises because a vortex, as an extended object, has internal degrees of freedom.

For a repulsive nucleus-vortex interaction, as found by Avogadro et al. (2007) and Avogadro et al. (2008), and (Wlazłowski et al. 2016), the vortex pins less strongly to the interstices of the lattice; see Fig. 3. For most lattice orientations, there is no pinning; the vortex is able to wiggle between the nuclei. Averaging over randomly chosen lattice orientations, we find:

$$f_p \simeq \frac{2 \times 10^{-4}}{3 \times 10^{16}} \left(\frac{|E_p|}{4 \text{ MeV}} \right) \left(\frac{b}{30 \text{ fm}} \right)^{-2} \begin{array}{l} \text{MeV fm}^{-2} \\ \text{dyn cm}^{-1} \end{array} \quad (5)$$

an order of magnitude smaller than for an attractive potential, a factor of ~ 30 larger than found by Seveso et al. (2016), and a factor of 30-300 smaller than estimated by Anderson & Itoh (1975) with a dimensional argument.

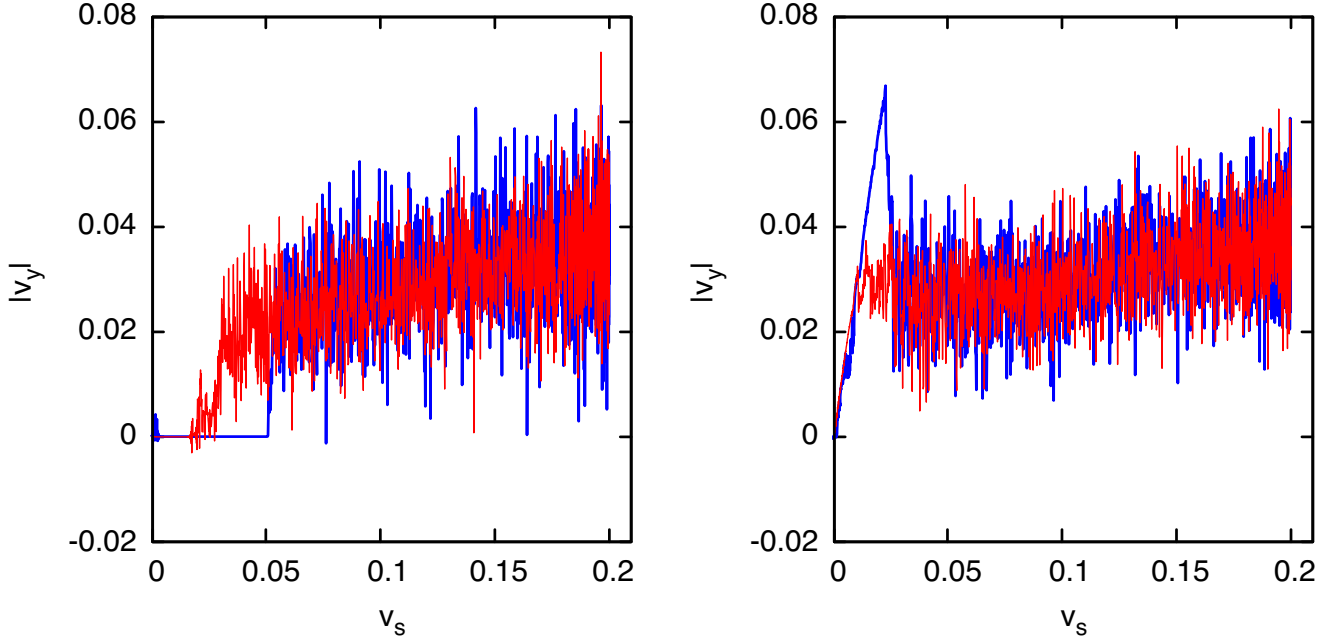


Figure 3. As in Fig. 2, for a repulsive nuclear potential. Typically, there is no pinning transition, as in the right panel. For favorable lattice orientations for which there is a sharp transition, the threshold force is somewhat lower than for an attractive potential.

As long as the lattice is regular, these results are not significantly changed for different symmetries; the results are similar for a face-centered cubic (fcc) lattice, or an alloy consisting of an fcc lattice and a displaced sub-lattice.

3.2. Impure lattice

The presence of impurities, such as dislocations or nuclei with different charge than their neighbors or mono-vacancies (missing nuclei), can substantially strengthen pinning for a repulsive lattice. In a repulsive lattice, mono-vacancies will attract the vortex. Fig. 4 shows examples for a dilute lattice of randomly distributed attractive impurities in a repulsive bcc lattice with $E_p = 2$ MeV. The pinning strength is now largely independent of lattice orientation as the pinning to impurities is stronger than to the repulsive lattice. Impurities have little effect in an attractive bcc lattice since the pinning to the nuclei is much stronger than the repulsive case.

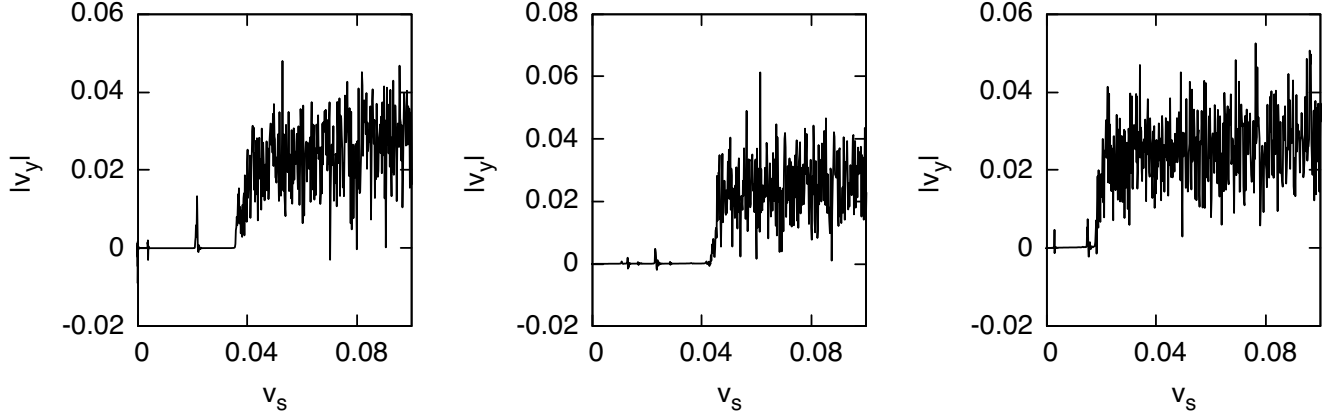


Figure 4. Pinning transitions in a repulsive bcc lattice with a dilute lattice of randomly placed attractive impurities for three orientations of the bcc lattice. Only v_s increasing with time is shown. The pinning strength is nearly independent of lattice orientation, and is determined by the density of impurities. For these examples $E_p = 2$ MeV, $\sigma_p = .3b$, the impurities are attractive with strength -2 MeV and density 0.02 per unit cell.

3.3. Nuclear Glass

As a model for the potential in a glass, we take

$$V(x, y, z) = \frac{E_p}{b} e^{-\left(\frac{b}{\sigma_p}\right)^2 [\phi(x) + \phi(y) + \phi(z)]}$$

with the phases given by random Fourier series of N modes:

$$\phi(x) = \frac{1}{N} \sum_{i=1}^N [c_i \sin(k_i x + \beta_i)]^2 \quad c_i = \text{rand}(), \quad k_i = k_0[\text{rand}() + .5], \quad \beta_i = 2\pi \text{rand}()$$

where $\text{rand}()$ is the from the interval $[0, 1]$, $k_0 = \pi/b$, and b is the mean distance between extrema in the potential. $\phi(y)$ and $\phi(z)$ are generated in the same way, with their own random numbers. We typically use $N = 5$. An example is shown in Fig. 5.

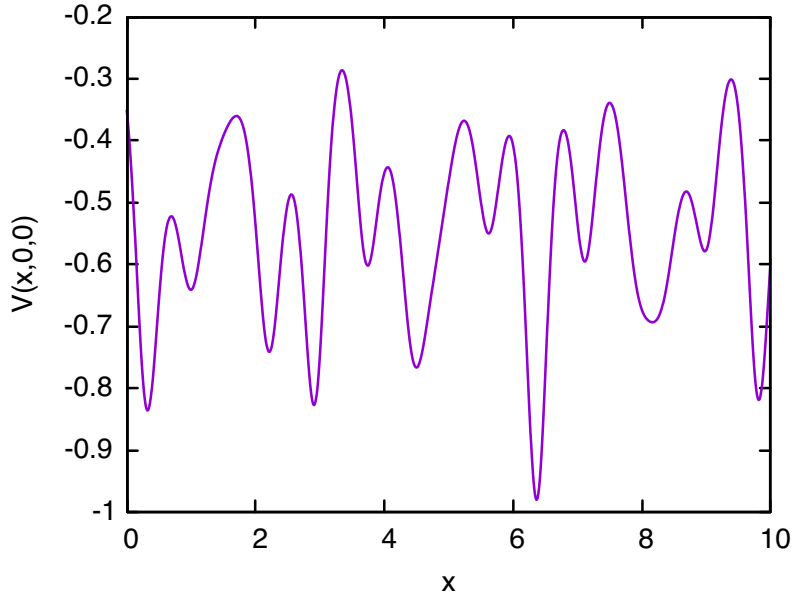


Figure 5. A slice through the random potential.

Pinning to a glass is nearly as strong as pinning to an attractive lattice for given E_p , and is independent of the sign of E_p . The hysteresis identified for other pinning situations is usually present, but not always; see Fig. 6. The pinning force per length is nearly equal to that of the attractive lattice (eq. 4).

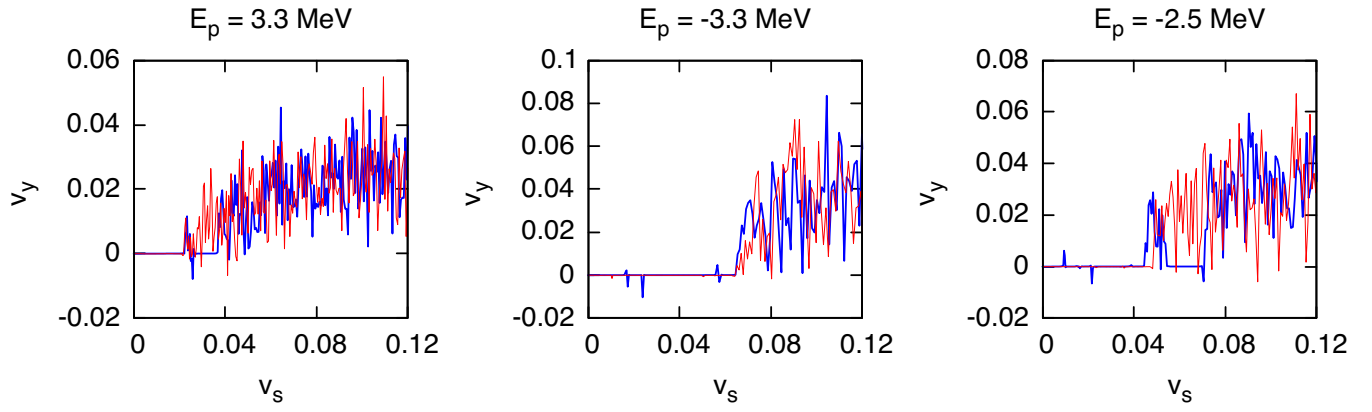


Figure 6. Examples of pinning in a glass. For these examples, $b = 30$ fm. The hysteresis identified previously is evident in the left and right plots, but not in the middle one. The first blue spike in the plot on the left is readjustment of the vortex, not unpinning.

A movie of vortex motion is shown in Fig. 7.

[Click here for animation](#)

Figure 7. Animation of a vortex forced through a repulsive glass. The coordinates and scalings are as in Fig. 1.

4. DISCUSSION

For an ideal bcc lattice, pinning occurs for some lattice orientations and is absent for others. For an attractive bcc lattice, the angle-averaged pinning force per unit length is $f_p \sim 10^{-3} \text{ MeV fm}^{-2} \sim 10^{17} \text{ dyn cm}^{-1}$, with a critical flow velocity for unpinning of $v_c = f_p/(\rho_s \kappa) \sim 10^{-4} c$. If the vortex-nucleus reaction is repulsive, as indicated by a number of calculations (Pizzochero et al. 1997; Donati & Pizzochero 2003, 2004, 2006; Wlazłowski et al. 2016), pinning in a bcc lattice is weakened somewhat to $f_p \sim 10^{-4} \text{ MeV fm}^{-2} \sim 10^{16} \text{ dyn cm}^{-1}$, with a critical flow velocity for unpinning of $v_c \sim 10^{-5} c$. If the nuclear lattice consists of large micro-crystals with different orientations, the pinning dynamics is likely very complex, with unpinned vortex segments exciting Kelvin waves that propagate along the vortex and unpin it elsewhere. Unpinned segments could pin as they move into regions where the lattice orientation is favorable for pinning. If the bcc lattice contains a dilute distribution of attractive impurities (*e.g.*, mono-vacancies), pinning occurs for any lattice orientation. If the nuclear lattice is amorphous, probably a better approximation of the lattice structure than the bcc idealization (Jones 2001; Kobayakov & Pethick 2014), the pinning is strong, independent of the sign of the vortex-nucleus interaction, with a pinning force per unit length of $f_p \sim 10^{-3} \text{ MeV fm}^{-2} \sim 10^{17} \text{ dyn cm}^{-1}$ (comparable to the angle-averaged pinning force in an attractive bcc lattice). Because a vortex is able to bend as it settles into the pinned state, the pinning force is much stronger than found by Seveso et al. (2016), who obtained the force by averaging over lattice orientations for straight vortices, effectively assuming that the vortex tension is infinite.

Is the pinning force strong enough to account for large spin glitches? Suppose the pinned vortices follow the rotation axis of the star of radius R in the crust of thickness $\Delta R \ll R$. The angular momentum in the superfluid available to drive a glitch is the excess above that for co-rotation of the superfluid with the crust. The velocity difference between the pinned superfluid and the crust is $v_s = f_p/\rho_s \kappa$, and the excess angular momentum in the inertial frame is

$$\Delta J_s = \int d^3r r \sin \theta \rho_s v_s \simeq 2\pi R^3 \Delta R \frac{\bar{f}_p}{\kappa}, \quad (6)$$

where \bar{f}_p is the mean pinning force in the crust. At the time of a glitch, suppose that all of this available angular momentum is given to the crust plus any other components (*e.g.*, part of the stellar core) that are tightly coupled together over the time scale of the glitch. Let the moment of inertia of the tightly coupled components of the star be fI , where I is the total moment of inertia of the star and f is the fraction of that moment of inertia that is tightly coupled. If the core is not decoupled by a glitch, then $f \sim 1$, while if the core is completely decoupled by the glitch $f \sim 10^{-2}$. (In the latter case, observed glitch recovery could represent response of the core.) The glitch magnitude is given by $I\Delta\Omega_c = \Delta J_s$, giving

$$\frac{\Delta\Omega_c}{\Omega_c} \simeq 2 \times 10^{-5} f^{-1} \left(\frac{R}{10 \text{ km}} \right)^4 \left(\frac{\Omega_c}{10^2 \text{ rad s}^{-1}} \right)^{-1} \left(\frac{I}{10^{45} \text{ g cm}^2} \right)^{-1} \left(\frac{\Delta R/R}{0.05} \right) \left(\frac{\bar{f}_p}{10^{16} \text{ dyn cm}^{-1}} \right) \quad (7)$$

Pinning is easily strong enough to account for glitches of magnitude $\Delta\Omega_c/\Omega_c = 10^{-6}$ for any $f \leq 1$.

We find the transition from the pinned state to the unpinned state to be generally very sharp, but it is possible that the transition occurs over a small range in v_s that we have not resolved in our simulations at zero temperature. At finite temperature T , the transition at critical velocity v_c is expected to be smoothed over a velocity range $\sim (kT/A)v_c$, where A is an activation energy in the range $kT < A < E_p$ (Link et al. 1993; Link 2014)⁴. If the transition occurs over some range in v_s , the slow increase in v_s (over the stellar spin-down time of $> 10^3$ yr), will not produce catastrophic vortex unpinning; rather, vortex segments will begin to move slowly, reducing v_s locally, and preventing the vortices from entering the ballistic regime. It would appear that a trigger is needed to produce large-scale vortex motion. One possible trigger is a starquake, resulting from relaxation of the crust as the star spins down. A starquake could cause a portion of the inner crust to move briefly at a speed comparable to that of shear waves in the matter ($\sim 10^8 \text{ cm s}^{-1}$), placing vortices on the supercritical side of the curve in Fig. 1. As the quake ends, v_s is restored to a sub-critical value, but the vortices are now following the upper, ballistic branch of the hysteresis curve. The ballistic vortices exert large drag on the crust until v_s is reduced to nearly zero, and a spin glitch occurs.

Our numerical experiments demonstrate that unpinning and repinning are: i) very sensitive to the lattice orientation, and, ii) not entirely deterministic for a given orientation. It seems inevitable that repeated unpinning and repinning would cause a long vortex line to deviate significantly from straight. At each pinning site, the vortex is bent by a small

⁴ This expectation should be checked with simulations.

angle $\theta \propto |E_p|/T_v$, but the directions of the kinks are likely to be somewhat random. The directions of neighboring vortex segments could differ significantly, so that the vortex array is tangled to some extent.

Suppose, during a glitch, a hot, unpinned vortex is driven close to a cold, pinned vortex. The repulsive force between the two vortices could cause the pinned vortex to unpin. We see in our simulations the propagation of Kelvin excitations along a single vortex. We suppose that, during a glitch, the macroscopic state of the vortex array can be described by an order parameter - an “activity” - that reflects the strength of the local vortex excitation. At the start of a glitch, the activity becomes high in a small region of the crust. The dispersion in the vortex directions in this region, combined with the transmission of excitations between the neighboring vortices, will cause activity to be transported in all directions, and not just along the mean direction of vorticity. This transport is likely to be anisotropic, akin to deflagration fronts in many realistic situations.

Finally, we note that transitions between pinned and unpinned states depend on the drag force on a moving vortex, an issue deserving further study.

Y. L. is supported by NSF Grant AST-2009453. The computations for this work were performed on the Hyalite High-Performance Computing Cluster at Montana State University, and on a desktop at the Flatiron Institute. The Flatiron Institute is a division of the Simons Foundation, supported through the generosity of Marilyn and Jim Simons. We thank Andrei Gruzinov for useful discussions.

APPENDIX

A. SOLUTION METHOD

Eq. 1 applies to first order in $\partial\mathbf{u}/\partial z$. In this limit, variations in the direction of $\boldsymbol{\kappa}$ do not enter to first order in the force in directions perpendicular to the vortex, and the vortex equation of motion becomes

$$T_v \frac{\partial^2 \mathbf{u}}{\partial z^2} + \rho_s \boldsymbol{\kappa} \hat{z} \times \left(\frac{\partial \mathbf{u}}{\partial t} - \mathbf{v}_s \right) - \eta \frac{\partial \mathbf{u}}{\partial t} + \mathbf{f} = 0. \quad (\text{A1})$$

Let the unit of length be the lattice spacing b , and define a time unit $\rho_s \kappa b^2 / T_v$ ($\sim 10^{-20}$ s in a neutron star). Define $\Psi \equiv u_x + iu_y$ and $\tilde{f} \equiv f_x + if_y$. Eq. A1 becomes

$$\frac{\partial^2 \Psi}{\partial z^2} + (i - \gamma) \frac{\partial \Psi}{\partial t} - iv_s = -\frac{\tilde{f}}{T_v} \quad (\text{A2})$$

where $\gamma \equiv \eta / \rho_s \kappa$ (dimensionless). For $\gamma = 0$, this equation becomes the one-dimensional Schrödinger equation.

We take the straight vortex to be of length L , and the moving vortex to be defined over the interval $z \in [0, L]$ with free ends. The boundary conditions are

$$\frac{\partial \Psi}{\partial z} = 0 \text{ at } z = 0 \text{ and } L. \quad (\text{A3})$$

We estimate the vortex tension from hydrodynamics; the vortex tension is the kinetic energy per unit length in the velocity field produced by the vortex. In cylindrical coordinates for a vortex at $r = 0$, the flow velocity is $\mathbf{v}_v = \hat{\phi} \kappa / 2\pi r$. Treating the vortex has a hollow core of radius the superfluid coherence length ξ , the tension is (see, *e. g.*, [Sonin \(1987\)](#)).

$$T_v = \frac{1}{2} \int d^2 \rho_s v_f^2 = \frac{1}{4\pi} \rho_s \kappa^2 \ln \frac{L_c}{\xi}, \quad (\text{A4})$$

where L_c is an upper cut-off for the integral. As a vortex moves through the lattice, it becomes bent over a length scale $10\text{-}1000b$; L_c is approximately the bending length in this small wavelength limit and $\ln L_c/\xi$ is typically ~ 3 ⁵. Numerically,

$$T_v \simeq 0.6 \left(\frac{\rho_s}{10^{13} \text{ g cm}^{-3}} \right) \text{ MeV fm}^{-1}, \quad (\text{A5})$$

⁵ In the opposite limit of long wavelength, the upper cut-off is comparable to the inter-vortex spacing, and the logarithmic factor is ~ 10 times larger ([Tkachenko 1966a,b,c, 1969](#); [Fetter 1967](#); [Baym & Chandler 1983](#)).

where a typical value of the unentrained superfluid mass density was used. Wlazłowski et al. (2016) have argued that the vortex tension could be significantly larger at high density than the value given by the hydrodynamic estimate. We take $T_v = 0.6 \text{ MeV fm}^{-1}$ when estimating numerical values. Our calculations are for fixed E_p/T_v , so a larger value of T_v implies a larger value of E_p .

We solve eq. A2 using a spectral method. Expand $\Psi(z, t)$ in a Fourier series

$$\Psi(z, t) = \sum_{n=0}^{\infty} a_n(t) \cos k_n z \quad k_n = \frac{n\pi}{L}. \quad (\text{A6})$$

This expansion obeys the free-end boundary conditions. The $n = 0$ mode corresponds to translation of the vortex. Substitute eq. A6 into eq. A2, and invoke orthogonality of $\cos k_n z$ over the domain to obtain an infinite sequence of coupled, ordinary differential equations

$$(i - \gamma)\dot{a}_n - k_n^2 a_n - i v_s \delta_{n0} = \tilde{f}_n(t) \quad n = 0.. \infty \quad (\text{A7})$$

where

$$\tilde{f}_n(t) = \frac{2b}{LT_v} \int_0^L dz \tilde{f}(z, t) \cos k_n z \quad n \geq 1, \quad (\text{A8})$$

and for the translational mode:

$$\tilde{f}_0(t) = \frac{b}{LT_v} \int_0^L dz \tilde{f}(z, t) \quad n = 0. \quad (\text{A9})$$

In numerical simulations, we use a finite number of modes N_m where N_m is determined by the desired spatial resolution; see below.

To evaluate the force, define a grid in z with spacing Δz

$$z_i = (i - 1)\Delta z \quad i = 1..N_z, \quad (\text{A10})$$

so $\Delta z = L/(N_z - 1)$. Eqs. A8 and A9 become

$$\tilde{f}_n = \frac{2\Delta z}{L} \sum_{i=1}^{N_z} M_{ni} F_i \quad (\text{A11})$$

$$\tilde{f}_0 = \frac{\Delta z}{L} \sum_{i=1}^{N_z} M_{0i} F_i \quad (\text{A12})$$

where M is an $N_m \times N_z$ matrix

$$M_{ni} = \cos k_n z_i, \quad (\text{A13})$$

and F_i is an N_z dimensional vector

$$F_i = \frac{b\tilde{f}(z_i)}{T_v}. \quad (\text{A14})$$

From eq. A6,

$$\Psi(z_i, t) = \sum_{n=0}^{N_m} a_n M_{ni}. \quad (\text{A15})$$

For the force at a point $\mathbf{r}(z, t) = \mathbf{u}(z, t) + \hat{z}z$ on the vortex:

$$\bar{\mathbf{f}}(\mathbf{r}, t) = -\nabla_{\perp} V(\mathbf{r}, t) \equiv -\hat{x} \frac{\partial V}{\partial x} - \hat{y} \frac{\partial V}{\partial y}. \quad (\text{A16})$$

To solve the system, we evaluate \bar{f}_n from eqs. A11 and A12 by matrix multiplication, advance the coupled equations in eq. A7 by a time step, and then use eq. A15 to transform back to coordinate space.

Typically $\Delta z \simeq 10^{-2}b$ gives sufficient resolution, so $N_z = 100L/b$. The highest wave number should be about $4\pi/b$, so that $N_m = 4L/b$. For $L = 100b$, $N_z = 10^4$ and $N_m = 400$.

To integrate eq. A7, we use best to use fifth-order Runge-Kutta with adaptive step size to control error.

REFERENCES

- Alpar, M. A. 1977, *Astrophys. J.*, 213, 527
- Alpar, M. A., Chau, H. F., Cheng, K. S., & Pines, D. 1996, *Astrophys. J.*, 459, 706

- Anderson, P. W., & Itoh, N. 1975, *Nature*, 256, 25
- Antonopoulou, D., Espinoza, C. M., Kuiper, L., & Andersson, N. 2017, *Mon. Not. Roy. Astr. Soc.*, 473, 1644
- Ashton, G., Lasky, P. D., Graber, V., & Palfreyman, J. 2019, *Nature Astronomy*, 3, 1143
- Avogadro, P., Barranco, F., Broglia, R., & Vigezzi, E. 2008, *Nuclear Physics A*, 811, 378
- Avogadro, P., Barranco, F., Broglia, R. A., & Vigezzi, E. 2007, *Phys. Rev. C*, 75, 012805
- Baym, G., & Chandler, E. 1983, *J. Low Temp. Phys.*, 50, 57
- Bransgrove, A., Beloborodov, A. M., & Levin, Y. 2020, *The Astrophysical Journal*, 897, 173
- Brown, E., & Cumming, A. 2009, *Astrophys. J.*, 698, 1020
- Cheng, K. S., Alpar, M. A., Pines, D., & Shaham, J. 1988, *Astrophys. J.*, 330, 835
- Donati, P., & Pizzochero, P. 2003, *Physical Review Letters*, 90, doi: [10.1103/PhysRevLett.90.211101](https://doi.org/10.1103/PhysRevLett.90.211101)
- Donati, P., & Pizzochero, P. M. 2004, *Nuclear Physics A*, 742, 363
- . 2006, *Phys. Lett. B*, 640, 74
- Epstein, R. I., & Baym, G. 1988, *Astrophys. J.*, 328, 680
- . 1992, *Astrophys. J.*, 387, 276
- Fetter, A. L. 1967, *Phys. Rev.*, 162, 143
- Howitt, G., Melatos, A., & Haskell, B. 2020, *Mon. Not. Roy. Astr. Soc.*, 498, 320
- Jones, P. B. 1990, *Mon. Not. Roy. Astr. Soc.*, 243, 257
- . 1992, *Mon. Not. Roy. Astr. Soc.*, 257, 501
- . 1997, *Phys. Rev. Lett.*, 79, 792
- . 1999, *Phys. Rev. Lett.*, 83, 3589
- . 2001, *Mon. Not. Roy. Astr. Soc.*, 321, 167
- Kobyakov, D., & Pethick, C. J. 2014, *Physical Review Letters*, 112, 112504
- Link, B. 2009, *Phys. Rev. Lett.*, 102, 131101
- Link, B. 2014, *ApJ*, 789, 141
- Link, B., & Epstein, R. I. 1991, *Astrophys. J.*, 373, 592
- . 1996, *Astrophys. J.*, 457, 844
- Link, B., Epstein, R. I., & Baym, G. 1993, *Astrophys. J.*, 403, 285
- Palfreyman, J. L., Dickey, J. M., Ellingsen, S. P., Jones, I. R., & Hotan, A. W. 2016, *The Astrophysical Journal*, 820, 64, doi: [10.3847/0004-637x/820/1/64](https://doi.org/10.3847/0004-637x/820/1/64)
- Pizzochero, P. M., Viverit, L., & Broglia, R. A. 1997, *Phys. Rev. Lett.*, 79, 3347
- Ruderman, M. 1991, *Astrophys. J.*, 382, 587
- Schwarz, K. 1977, *Physical Review Letters*, 38, 551
- . 1978, *Physical Review B*, 18, 245
- Seveso, S., Pizzochero, P. M., Grill, F., & Haskell, B. 2016, *Mon. Not. Roy. Astr. Soc.*, 455, 3952
- Sonin, E. B. 1987, *Rev. Mod. Phys.*, 59, 87
- Tkachenko, V. K. 1966a, *Sov. Phys. JETP*, 22, 1282
- . 1966b, *Sov. Phys. JETP*, 23, 1049
- . 1966c, *Zh. Eksp. Teor. Fiz.*, 50, 1573
- . 1969, *Sov. Phys. JETP*, 29, 245
- Warszawski, L., & Melatos, A. 2008, *Mon. Not. Roy. Astr. Soc.*, 390, 175
- . 2011, *Mon. Not. Roy. Astr. Soc.*, 415, 1611
- . 2013, *Monthly Notices of the Royal Astronomical Society*, 428, 1911
- Warszawski, L., Melatos, A., & Berloff, N. G. 2012, *Phys. Rev. B*, 85, 104503
- Wlazłowski, G., Sekizawa, K., Magierski, P., Bulgac, A., & Forbes, M. M. 2016, *Physical Review Letters*, 117, 232701